Mt. St. Helens' Aerosols: Some Tropospheric and Stratospheric Effects

J. J. MICHALSKY AND G. M. STOKES

Pacific Northwest Laboratory, Richland, WA 99352

(Manuscript received 23 October 1982, in final form 24 January 1983)

ABSTRACT

Aerosol optical depth measurements based on the attenuation of direct solar radiation before and after the six major explosive eruptions of Mt. St. Helens during 1980 are presented. These automated measurements are from a site 200 km mostly east and slightly north of the volcano. From the analysis it was concluded that in several cases the conversion of sulfur gases to sulfates proceeded much more rapidly (hours) than is usually found for tropospheric conditions. A possible explanation may be the greater availability of OH due to the presence of substantial water in the plume. The second major result of the analysis was that there was no evidence of a residual aerosol burden. Turbidity data taken between eruptions in 1980 were virtually identical in terms of magnitude and wavelength dependence to 1979 turbidity.

1. Introduction

Aerosols are concentrated primarily in two layers in the earth's atmosphere. The lower, tropospheric layer is the most familiar to us. Aerosols in this layer are readily perceived by their effect on our ability to see distant objects. These tropospheric particles are concentrated in the boundary layer which lies near the earth's surface. The other layer, with which we are less familiar and which was discovered only 20 years ago, is the stratospheric layer (Junge *et al.*, 1961). During volcanic episodes this layer is enhanced such that the total optical thickness may become comparable to that of its lower counterpart (Toon and Pollack, 1980).

Deviations from the mean optical properties of the stratospheric and tropospheric aerosols may have a significant climatic effect (Toon and Pollack, 1980). In the troposphere the optical depth at visible wavelengths and the single-scattering albedo are the primary optical properties that influence temperature and therefore climate. Introducing aerosols to this layer increases scattering, effectively increasing the albedo, and, therefore, cooling the troposphere. Above a critical single-scattering albedo, a net amount of visible radiation is returned to space which causes a cooling of the troposphere. Below this critical value enough energy is absorbed in this layer that the troposphere and the surface, with which it is in thermal contact, warm. The stratospheric aerosol layer (near 20 km) has a rather different effect than does the tropospheric layer. The response to an optical depth increase is similar for the stratosphere and troposphere, i.e., cooling occurs because of an effective albedo increase. However, the value of the single-particle scattering albedo is not important. Whether the radiation is scattered or absorbed by the stratospheric aerosols, they are not in thermal contact with the surface, and, therefore, these aerosols cause cooling for all values of the single-scattering albedo. Size is quite important, however, in the cool stratosphere. Small particles do not effectively block the escape of infrared radiation from the earth, while larger particles with diameters ≥ 1 μm do. Enough blocked radiation is reradiated to the surface for these sizes to cause a net warming.

In the troposphere the distribution of aerosols is non-uniform both spatially and temporally. Changing meteorological conditions and the particular mix of aerosol sources lead to significant changes in aerosol optical properties. Even with a stable atmosphere, the effects of aerosols would differ depending on the albedo of the underlying surface. Aerosols change the effective albedo of the earth, which, for a given aerosol, can mean a decrease in temperature if the surface is dark or an increase if the surface is bright. Climate calculations for simplicity consider time and space averages of tropospheric aerosol properties to predict expected temperature changes.

The stratosphere generally contains a more stable and uniform aerosol layer. It is composed mainly of sulfuric acid formed from gaseous sulfur compounds transported into the stratosphere from the troposphere (Crutzen, 1976). Photochemistry and solution chemistry slowly generate a mostly stable and fairly uniform aerosol layer. This stability is upset by volcanic eruptions which introduce large numbers of aerosols in the form of tephra and aerosol precursors, i.e., sulfur gases. While the tephra tend to be large and fall out rather quickly, in days to weeks, the sulfur gases evolve to sulfuric acid droplets rather slowly and, hence, can maintain an appreciable aerosol layer

in the stratosphere for two to three years after an eruption.

Two potentially major influences on climate are the trace gas buildup (CO_2 as well as others) and solar luminosity changes. These both may have greater potential for long-term climate impact than do volcanoes; however, volcanic effects, since they are well defined in time, provide a suitable test of climate perturbation. Understanding the aerosol influence on climate may be especially important because an increase in volcanic activity which would lead to cooling may temporarily mask the effects of an expected warming due to CO_2 increase until the CO_2 burden is out of control (Hansen *et al.*, 1981).

In this paper we examine the influence Mount St. Helens has had locally on the amount and characteristics of the aerosols during 1980 relative to the previous year. Most of our discussion concerns the troposphere, but we make estimates of the stratospheric effect as well.

2. Methodology

Solar radiation is attenuated in the earth's atmosphere according to

$$I_\lambda = I_{0\lambda} \exp(-\tau_\lambda m), \tag{1}$$

where I_λ is the spectral irradiance at a fixed point in the atmosphere at wavelength λ, $I_{0\lambda}$ is the spectral irradiance at this wavelength at the top of the atmosphere, m is the equivalent air mass in the direction of the sun normalized to the air mass in the zenith direction, and τ_λ is the optical depth in the zenith direction. Eq. (1) may be linearized by taking the logarithm. This leads to

$$\ln I_\lambda = \ln I_{0\lambda} - \tau_\lambda m. \tag{1a}$$

The slope of the best straight line obtained by fitting in a least-squares sense to a plot of the logarithm of the measured intensity versus air mass is just equal to the optical depth. The optical depth τ (dropping the subscript λ) can be written as the sum of four components, i.e.,

$$\tau = \tau_a + \tau_o + \tau_R + \tau_m,$$

where the subscripts denote aerosol, ozone, Rayleigh and molecular optical depths, respectively; τ_o, τ_m and τ_R are taken as knowns and can be subtracted leaving us with the optical depth due to aerosol at as many wavelengths as we have filters. Actually, in filter radiometry of the type described here the filter passbands have been selected to avoid virtually all molecular absorption with the exception of ozone. This makes the molecular contribution negligible and means that only correction for the Chappuis bands of ozone must be applied to the data in practice.

Aerosols > 0.1 μm often have been parameterized by a size distribution represented as

$$dN/d\log r = Cr^{-\nu} \tag{2}$$

(Junge, 1963) or, alternatively, as

$$dN/dr = (C/\ln 10) r^{-\nu-1}.$$

In the limit that the contribution to the extinction from particles very much larger and very much smaller than ~ 0.5 μm can be ignored, it can be shown that

$$\tau_a = C^* \lambda^{-\nu+2},$$

or more commonly

$$\tau_a = \beta \lambda^{-\alpha}. \tag{3}$$

Taking the logarithm of both sides of this equation yields

$$\log \tau_a = \log \beta - \alpha \log \lambda.$$

Again we have a linear equation, the slope of which is related to the size distribution of the aerosols if that size distribution is described approximately by the power law given by Eq. (2). For particles much smaller than λ, α approaches 4, i.e., the Rayleigh value. For particles much larger than λ, α approaches 0 as the particles become neutral attenuators. The mean value of α for continental air is 1.3 ± 0.2 (Angstrom, 1961).

3. Observations

Our measurements are made using a computer-controlled scanning photometer (Kleckner *et al.*, 1981). Direct solar radiation is measured through 12 filters with a field-of-view of 1.5°. The 12-filter measurement set is repeated every 5 mins from sunrise to sunset. Observations began in the Spring of 1978 and still continue. The data presented are from one of nine North American photometer sites. The data chosen are from Richland, Washington, some 200 km mostly east and slightly north of Mount St. Helens. The 12 filters with which measurements are made are given in Table 1. Only five (those with asterisks) are used in the reported data although nine (four more with double asterisks) are of potential use. Two are contaminated by water vapor and/or molecular oxygen and the twelfth is not blocked sufficiently in the infrared for use with a silicon photodiode detector. The five filters chosen are narrow and fairly well span the wavelength response of the detector. Three of the four filters which could have been used have broad passbands, and the fourth has a very slight molecular oxygen contamination. We have, in fact, used all nine to check our results based on the five filters. Incorporating them has little effect in most cases. Exceptions are the low optical depth cases when the log τ versus log λ relationship is rather poorly defined.

The stability of the photometer's detector and data recording system is better than 1% as described in

Kleckner *et al.* (1981). The optical elements of the instrument are less stable in the long term and problems such as solarization and interference filter instability are well known. However, in this measurement the optical depth is obtained from the ratio of the change in the logarithm of the intensity to the change in air mass in a typical time of two to three hours requiring stability over that period only.

Fig. 1 is an example of the log optical depth versus log wavelength plots generated when all 12 filters are used (a) and when only the five narrow filters are plotted (b). The general properties of the filters and the sources of contamination are indicated in Fig. 1 and Table 1. A plot of aerosol optical depth at 530 nm versus time of year for 1980 from the initial low-amplitude eruption on 27 March to two weeks following the last explosive event on 17 October appears in Fig. 2. Table 2 contains these data plus ancillary information. There was some concern that the day-to-day comparisons reflect that variability and not the diurnal patterns, perhaps associated with convection cells caused by solar heating (Peterson *et al.*, 1981). For the most part we have confined our comparisons to data taken in the morning or evening between two and five air masses. When data do not exist, we relax these tolerances somewhat in order to have more complete coverage. When tracking an event, such as the intrusion of volcano-related aerosols, we use all of a day's data. The average air mass is the mean of the points used in the least-squares determination of the total τ's using Eq. (1a). The correlation coefficient R (Bevington, 1969) gives a sense of how linear the relationship between log τ_a and log λ is, or, said another way, how well the size distribution approximates a power law; for values of $R > 0.96$ we cannot indicate how well correlated those variables are, but

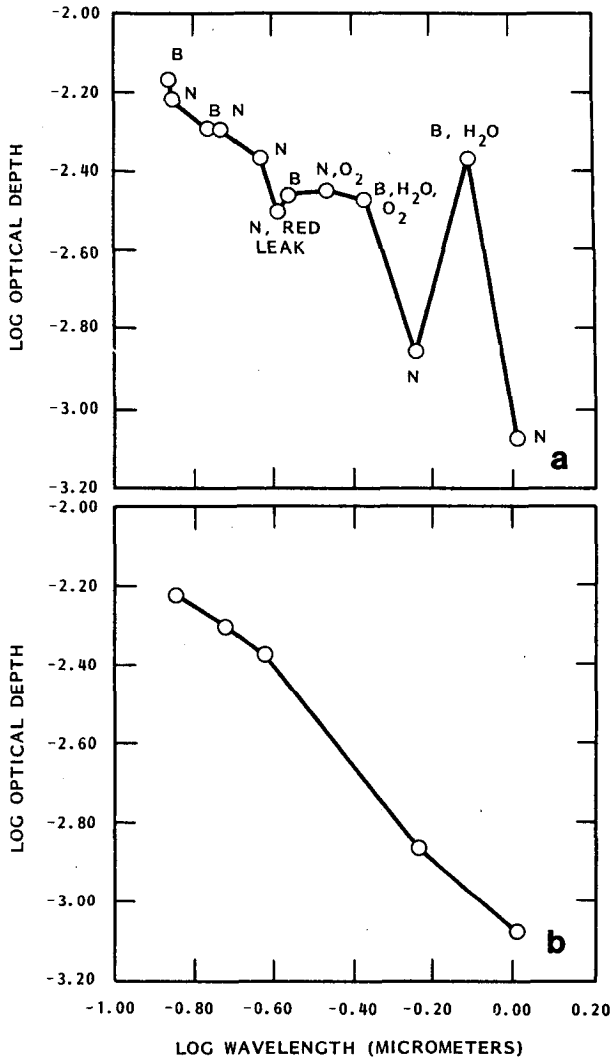

FIG. 1. The natural logarithm of the optical depth due to aerosols as a function of the natural logarithm of the wavelength in micrometers for all twelve filters (a) and for the five narrow, uncontaminated filters (b).

TABLE 1. Solar photometry filters

Filter No.	Central wavelength (nm)	Bandpass (nm)	Characteristics
1	395.0**	60	Broad
2	427.8*	1	OK
3	470.0**	100	Broad
4	486.1*	2	OK
5	535.0*	3	OK
6	557.7	1	Probable red leak
7	570.0**	100	Broad
8	630.0**	1	Slight contamination from O_2 absorption
9	680.0	120	O_2, H_2O absorption contamination
10	785.0*	20	OK
11	900.0	160	H_2O absorption contamination
12	1010.0*	30	OK

* Used for aerosol analysis.
** Usable for aerosol analysis but not used for Table 2 results.

rather that a chance occurrence of a value of R this large from a random distribution is less than 1%. The plume overflight probability is based on a trajectory analysis of the wind flow patterns at 700 mb pressure which is approximately the pressure at the summit of Mt. St. Helens. The winds are based on rawinsonde measurements which commence daily at 0000 and 1200 GMT or 0400 and 1600 PST. The dilution of the plume is not assessed; nor are the trajectories at higher or lower levels, which may contribute to the overlying layers considered at Richland. The SO_2 released by Mt. St. Helens is based on data taken with an airborne correlation spectrometer (Casadevall *et al.*, 1981). There are large errors associated with an individual measurement, hence the trends are more indicative of the abundance of SO_2 emitted.

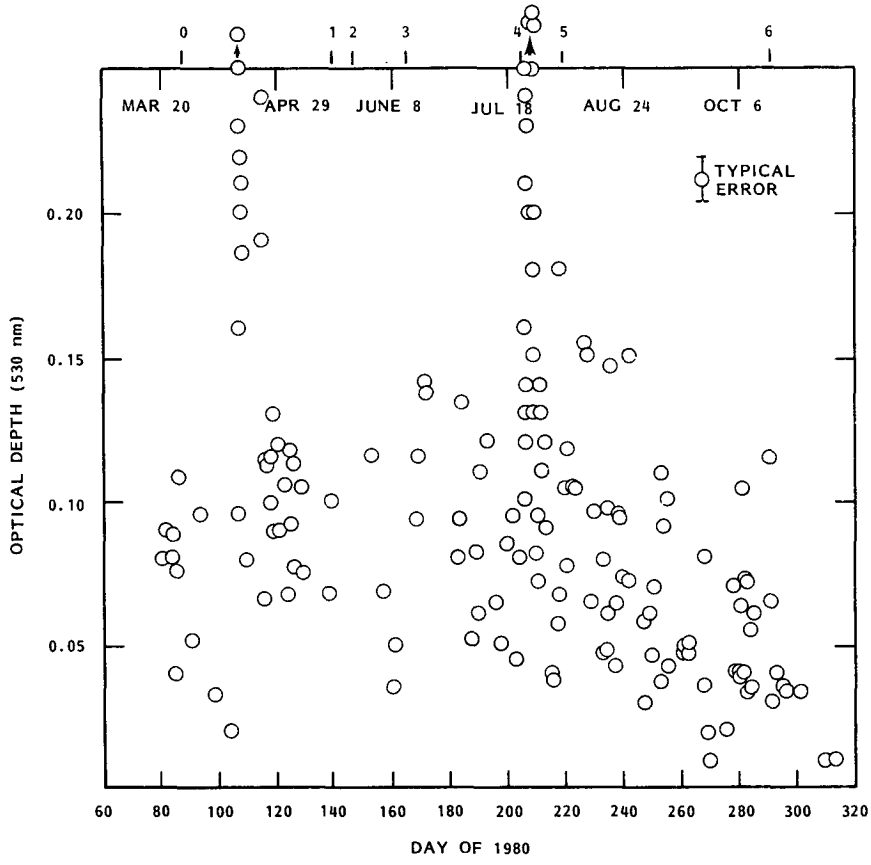

FIG. 2. The optical depth due to aerosols at 530 nm as a function of day of 1980.

On two of the six eruptions, indicated in Fig. 2, Richland received ash deposits. These were following the 18 May (Day 139) and 22 July (Day 204) eruptions. Cloudy weather with rain above seasonal norms followed the initial and largest eruption on 18 May. As a result, little turbidity data were collected for over a month, but what data there were appeared to be about that expected for May and June. Clear weather preceded and followed the 22 July eruption and resulted in a very good data set defining the volcanic event. A large increase in turbidity for about a week following that eruption is clearly shown in Fig. 2. There is no clearly associated increase in turbidity after any of the other major eruptions.

One aspect of Fig. 2 not associated with the major events stands out. On the afternoon of 15 April (Day 106) the optical depth increased by a factor of 2 or more above typical seasonal values. The optical depths were large for more than 24 h. Six days later the values were up again to comparable levels. If we examine this event, we find that the wavelength dependence is indicative of scattering from large particles on the 15th and 16th, and the size distribution on the 23rd tends to favor larger particles somewhat. The initial low-amplitude eruption phase was between 27 March and 22 April. Since there are unconfirmed reports of ashfall as far away as Spokane, Washington during this period, the data may reflect the passage of a well-defined ash cloud during that period in April. The wind trajectory analysis indicates in Table 2 that this interpretation is not excluded.

The most interesting subset of these data is the one centered about two weeks before and after the 22 July eruption. The clear weather allowed us to establish a baseline before the eruption and track the volcano's local influence on aerosol loading well after the event. Fig. 3 is a plot of the optical depth at 530 nm and the wavelength exponent of Eq. (3) versus time of year before and after the 22 July event. The eruption occurred in the late afternoon of that day. The increase in optical depth was marked by a peak near Day 208 and then a decrease to typical seasonal values by Day 210. There was a change in the wavelength dependence of the aerosol attenuation (α) during this 6-day period which was not correlated with the turbidity increase. The day following the eruption showed an increase in optical depth and a decrease in the wavelength exponent α which is in accord with our expectations of large ash particles associated with the 22 July event. However, as the attenuation con-

TABLE 2. 1980 aerosol and related data.

Day	Average air mass	R	α	τ (535 nm)	Plume overflight probability	SO_2 released (tons day^{-1})
81.7	2.6	0.98	1.16	0.079 ± 0.009		
82.7	2.6	0.96	0.63	0.089 ± 0.006		
83.8	1.6	0.97	1.16	0.08		
84.0	2.6	0.99	1.37	0.087 ± 0.006		
84.7				0.040 ± 0.005		
85.7				0.075 ± 0.014		
86.0	2.5	1.00	0.84	0.108 ± 0.004		
90.7	2.5	0.97	1.39	0.052 ± 0.004	No	3–10
93.7	2.5	0.99	1.78	0.095 ± 0.006	No	3–10
98.7				0.033 ± 0.006	Possible	30
103.8				0.02	Probable	30
106.7	2.3	0.96	0.35	0.096 ± 0.008	Probable	0
106.8				0.16	Probable	0
106.9	1.3	0.96	0.38	0.23	Probable	0
107.0	1.9	0.97	0.48	0.532 ± 0.061	Probable	0
107.7	2.3	1.00	0.27	0.218 ± 0.006	Possible	0
107.8				0.21	Possible	0
107.9	1.4	0.97	0.31	0.20	Possible	0
108.0	2.7	0.96	0.45	0.186 ± 0.006	Possible	0
109.7				0.079 ± 0.008	No	0
114.6	2.7	1.00	0.91	0.19	Possible	10
114.8	1.3	0.99	1.11	0.24	Possible	10
115.6				0.066 ± 0.005	No	10
116.0				0.114 ± 0.005	No	10
116.7	2.3	0.96	0.57	0.110 ± 0.003	No	10
117.7	2.3	0.99	1.08	0.099 ± 0.003	No	10
118.0	2.2	1.00	0.74	0.118 ± 0.005	No	10
118.7	2.3	1.00	0.48	0.130 ± 0.005	No	10
119.0	2.3	0.98	0.58	0.089 ± 0.004	No	10
120.7	2.3	0.98	0.73	0.119 ± 0.007	Probable	10
121.0	2.9	0.99	0.78	0.090 ± 0.011	Probable	10
122.6	2.6	0.99	1.71	0.105 ± 0.006	No	10
124.1	3.5	0.99	1.27	0.067 ± 0.014	No	10
124.7	2.2	0.99	1.07	0.117 ± 0.003	Yes	10
125.0	2.2	0.99	1.02	0.092 ± 0.006	Yes	10
125.7	2.3	1.00	1.02	0.112 ± 0.005	No	10
126.0	2.3	0.98	0.99	0.078 ± 0.005	No	10
128.6	2.5	0.99	1.19	0.104 ± 0.008	Possible	50
129.0	2.2	1.00	1.28	0.074 ± 0.004	Possible	50
138.0	2.2	0.99	1.26	0.068 ± 0.008	Possible	15
139.0	2.8	0.98	1.08	0.099 ± 0.006		
152.6	2.2	1.00	1.19	0.115 ± 0.005	No	130
156.6				0.068 ± 0.004	No	260
160.1				0.035 ± 0.012		
160.7	2.2	1.00	1.03	0.049 ± 0.004	No	600
168.0	2.4	0.99	1.32	0.093 ± 0.004	No	1000
168.6	2.7	1.00	1.35	0.115 ± 0.010	No	1000
171.0	2.1	1.00	1.15	0.141 ± 0.007	Possible	1000
171.7	1.8	1.00	0.80	0.137 ± 0.006		
171.9	1.1	0.98	0.49	0.15		
182.8				0.08	Yes	1300–2600
183.0	2.1	0.99	1.11	0.093 ± 0.003	Yes	1300–2600
183.6	2.5	0.99	1.03	0.085 ± 0.005	Yes	2600
184.0	2.2	1.00	1.31	0.134 ± 0.004	Yes	2600
187.6				0.052 ± 0.010	Possible	2600
189.1	2.7	1.00	1.28	0.082 ± 0.010	Possible	1800
189.6	2.6	0.97	1.18	0.061 ± 0.004	No	2000
190.6				0.109 ± 0.008	No	2200
193.0	2.2	1.00	0.87	0.121 ± 0.009	No	1600
195.7	2.2	0.97	0.79	0.065 ± 0.003	No	1900
197.6				0.050 ± 0.009	Possible	880
198.0	2.1	0.98	0.87	0.064 ± 0.005	Possible	880
199.7	2.2	1.00	1.30	0.084 ± 0.006	Possible	1000
201.6	2.9	1.00	1.29	0.094 ± 0.007	No	1200
202.7				0.045 ± 0.003	No	1500

TABLE 2. (*Continued*)

Day	Average air mass	R	α	τ (535 nm)	Plume overflight probability	SO_2 released (tons day^{-1})
204.0	2.1	0.99	1.29	0.079 ± 0.004	Probable	1900
205.6	3.2	0.97	0.37	0.16	Yes	800
205.7				0.10	Yes	800
205.8				0.13	Yes	800
205.9				0.22	Yes	800
206.0				0.12	Yes	800
206.1				0.14	Yes	800
206.7	1.4	0.98	0.86	0.20	Yes	2000
206.8	1.2	0.98	0.99	0.20	Yes	2000
206.9	1.2	0.99	1.06	0.25	Yes	2000
207.0	2.3	0.99	1.02	0.23	Yes	2000
207.1	4.8	1.00	1.07	0.20	Yes	2000
207.6	2.9	1.00	1.32	0.35	Probable	1800
207.7	1.5	1.00	1.33	0.29	Probable	1800
207.8	1.2	1.00	1.74	0.29	Probable	1800
207.9	1.2	0.99	1.70	0.33	Probable	1800
208.0	1.5	1.00	1.61	0.37	Probable	1800
208.1	3.0	0.99	1.60	0.37	Probable	1800
208.6	2.7	1.00	1.50	0.25	Possible	1800
208.7	1.8	1.00	1.66	0.20	Possible	1800
208.8	1.2	1.00	1.92	0.18	Possible	1800
208.9	1.6	1.00	1.65	0.15	Possible	1800
209.0	2.0	1.00	1.58	0.15	Possible	1800
209.1	4.4	1.00	1.30	0.13	Possible	1800
209.7	2.2	0.97	0.92	0.081 ± 0.008	Probable	700
210.0	2.1	0.98	0.72	0.095 ± 0.007	Probable	700
210.7	2.2	0.96	0.65	0.072 ± 0.005	Yes	700
211.0	2.2	1.00	0.91	0.140 ± 0.004	Yes	700
211.7	1.8	0.97	0.57	0.11	Yes	1100
212.0	1.9	0.99	0.60	0.13	Yes	1100
212.7				0.09	Yes	900
212.9	1.3	0.97	0.60	0.12	Yes	900
215.0				0.04	Yes	1000
215.6				0.037 ± 0.005	Yes	1100
216.6	2.7	0.99	1.42	0.058 ± 0.005	No	1100
217.0	2.2	0.98	0.89	0.055 ± 0.003	No	1100
217.7	2.2	1.00	0.88	0.067 ± 0.004	No	930
218.0	2.2	0.99	0.52	0.180 ± 0.004	No	930
219.7	2.2	0.99	1.42	0.104 ± 0.005	Possible	780
220.6	2.6	0.98	1.10	0.078 ± 0.008		
221.0	2.2	0.98	0.80	0.118 ± 0.004		
222.6	3.5	1.00	1.08	0.105 ± 0.009	Possible	2000
223.7	2.3	1.00	0.99	0.102 ± 0.005		
226.6	2.6	0.99	1.23	0.154 ± 0.008	Possible	3400
227.0	2.6	1.00	1.79	0.335 ± 0.031	Possible	3400
227.8	1.3	0.99	1.70	0.15	Probable	1600
228.7	2.2	0.99	1.29	0.064 ± 0.007	No	760
229.7	2.3	0.98	0.62	0.096 ± 0.006		
232.7				0.047 ± 0.005	No	1300
233.0	2.2	0.97	1.02	0.078 ± 0.005	No	1300
233.7	2.3	0.98	0.90	0.048 ± 0.005	No	1900
234.0	2.3	1.00	1.18	0.097 ± 0.002	No	1900
234.7	2.3	0.98	1.11	0.061 ± 0.004	Possible	2600
234.9	1.3	0.98	1.10	0.06	Possible	2600
235.7	2.3	1.00	1.29	0.146 ± 0.008	Possible	2000
237.0	2.3	0.98	0.77	0.065 ± 0.009	Possible	1800
237.7	2.3	0.99	0.96	0.042 ± 0.005	Possible	1200
238.0	2.3	0.99	0.99	0.095 ± 0.006	Possible	1200
239.0	2.3	1.00	1.15	0.091 ± 0.005	Possible	530
239.7				0.074 ± 0.005		
241.7	2.7	0.97	1.41	0.071 ± 0.004		
242.0	2.7	0.99	1.49	0.15		
247.0	2.4	0.99	1.17	0.057 ± 0.011	Yes	1200
247.6				0.03	No	1200
248.7				0.061 ± 0.007	Probable	900

TABLE 2. (*Continued*)

Day	Average air mass	R	α	τ (535 nm)	Plume overflight probability	SO_2 released (tons day^{-1})
249.6				0.047 ± 0.005	Yes	600
250.0				0.033 ± 0.005	Yes	600
250.8	1.4	0.99	1.50	0.07	No	1300
252.7				0.038 ± 0.004	No	1800
253.0	2.5	0.99	0.72	0.110 ± 0.005	No	1800
253.7	2.5	1.00	1.29	0.091 ± 0.004	No	1000
254.0	2.5	1.00	1.20	0.097 ± 0.008	No	1000
255.7	2.6	0.97	1.57	0.043 ± 0.007	Possible	300
260.7				0.046 ± 0.006	No	500
261.0				0.051 ± 0.005	No	500
261.7				0.045 ± 0.009	Possible	600
262.0	2.6	0.96	1.02	0.049 ± 0.008	Possible	600
267.7	2.4	0.96	0.90	0.035 ± 0.010	No	720
268.0	2.7	1.00	0.94	0.091 ± 0.009	No	720
269.0	3.0	1.00	0.80	0.019 ± 0.004		
269.7				0.01		
275.7				0.023 ± 0.006	No	1400
276.0				0.014 ± 0.008	No	1400
277.7	2.7	0.98	1.16	0.072 ± 0.006	Possible	1600
278.0	2.8	0.99	1.65	0.041 ± 0.007	Possible	1600
279.0				0.041 ± 0.004	Yes	550
279.7				0.037 ± 0.011	Probable	500
280.0	2.9	0.96	1.42	0.038 ± 0.003	Probable	500
280.7	2.9	0.98	1.15	0.062 ± 0.008	No	470
281.0	3.3	1.00	1.72	0.104 ± 0.006	No	470
281.7	3.1	1.00	1.23	0.076 ± 0.003	Possible	800
282.0	3.4	1.00	1.71	0.071 ± 0.004	Possible	800
282.7				0.028 ± 0.005	Yes	760
283.7	2.8	0.98	0.52	0.034 ± 0.005	Possible	800
284.0				0.049 ± 0.007	Possible	800
284.7	3.2	0.99	0.99	0.060 ± 0.009	No	760
290.7	4.2	0.99	1.77	0.114 ± 0.009		
291.5	3.3	0.96	1.59	0.074 ± 0.012		
291.7				0.029 ± 0.004		
292.9				0.04		
295.7	3.0	0.96	1.33	0.036 ± 0.010		
296.7				0.032 ± 0.008		
301.7	3.2	0.96	1.96	0.034 ± 0.004		
309.7				0.01		
312.2				0.01		

tinued to increase, α began to increase and continued to increase after the extinction peak; α finally returned to values more typical of the summer season.

The largest optical depths during this event were associated with large α's. (Recall that the large α's are indicative of a preponderance of small particles.) The source of this increased small particle component may be the conversion of SO_2 released during this time. SO_2 was released in copious amounts during the period, approaching values of 2000 tons per day [Casadevall *et al.*, 1981 (see Table 2)]. Supporting this interpretation is the wind trajectory analysis for the period that suggests that Mt. St. Helens' plume was near the Richland station during most of the period. The drawbacks to this interpretation are prior suggestions that the conversion of SO_2 to sulfates proceeds much more slowly than the few hours it takes for the 200 km trip from Mt. St. Helens to the observing site [see Alkezweeny and Powell (1977) for a review of these estimates]. On the other hand, Pollack (1981) reviews the evidence for a rapid conversion of SO_2 to H_2SO_4 following the 18 May eruption in the vicinity of Mt. St. Helens. Since the speed of the conversion depends on the availability of the OH radical, perhaps the greater availability of hydroxyl may allow this transformation to proceed rapidly. A possible source of the hydroxyl may be water vapor released along with the SO_2. While this is a plausible explanation, it does not explain all of the data. Many times when conditions were favorable for the observations of large optical depths of small particles, i.e., large SO_2 releases from Mt. St. Helens with the plume supposedly overhead, we did not observe extraordinary optical depths or a steep wavelength dependence of the aerosol. Dispersion of the plume, reduced SO_2 to sulfate conversion, or inaccurate trajectory anal-

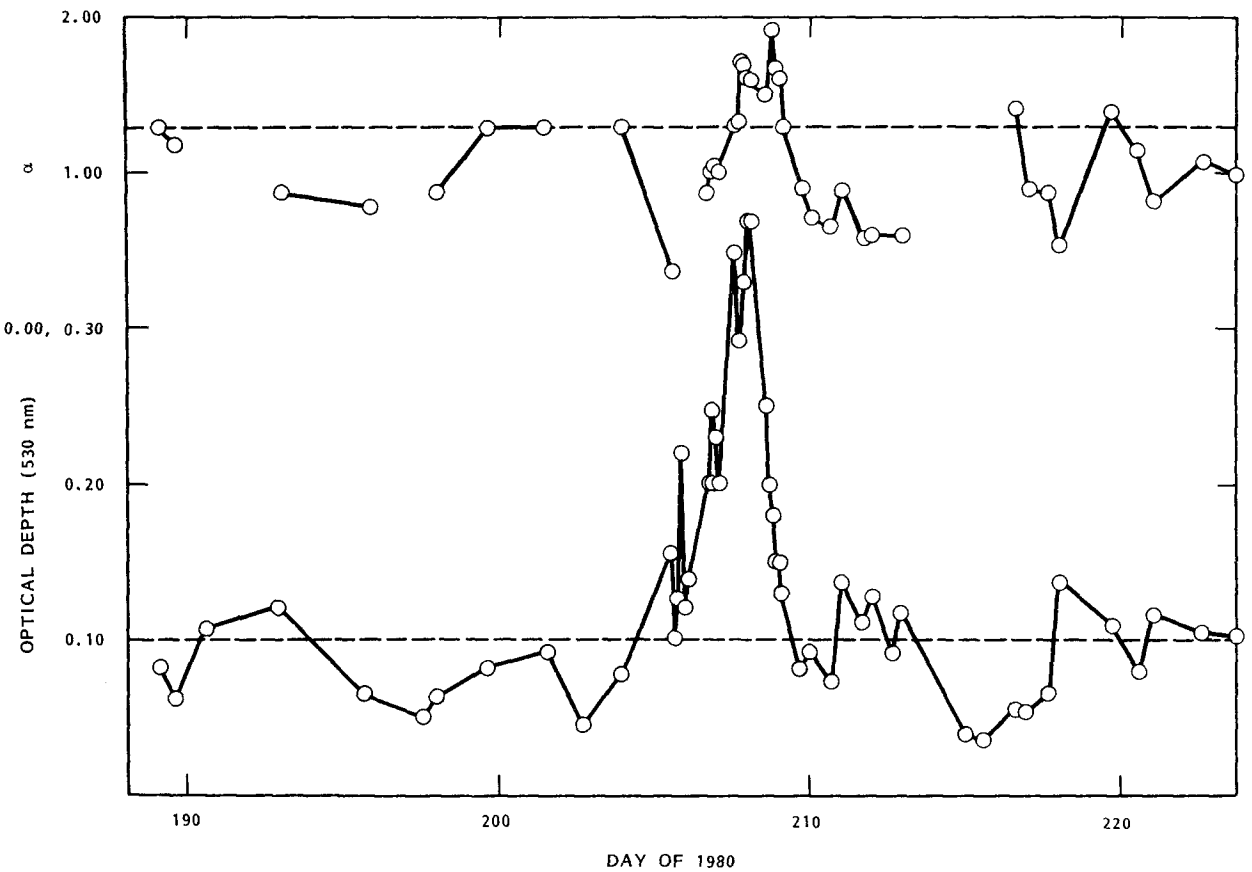

FIG. 3. The optical depth due to aerosols at 530 nm as a function of day of 1980 centered on the 22 July eruption (bottom) and the wavelength exponent of Eq. (3) as a function of day of 1980 (top).

yses are possible explanations. On the other hand, we generally observe a large α and a large optical depth when the plume is overhead (see Table 2).

Turbidity data taken during the volcanically quiescent periods of 1980 are also presented in Fig. 2 and Table 2. These data may be compared with seasonal data from the previous year to examine the residual effects of Mt. St. Helens on atmospheric transparency. Unpublished data taken in 1979 between 14 July and 7 October at the Richland site were found to have a mean optical depth of 0.081 ± 0.006 at 500 nm with a wavelength exponent of 1.19 ± 0.04. During that same period in 1980, excluding the 11 days following the 22 July eruption, the mean optical depth at 535 nm was 0.070 ± 0.004 with a wavelength exponent of 1.16 ± 0.04. This implies from Eq. (3) an optical depth at 500 nm of 0.075. Clearly, there is no meaningful change in the mean optical depth or its wavelength dependence between the two years. In fact, 1980 had a lower mean although it is within the error bounds set by the two data sets. It would appear that based on this comparison any aerosol or aerosol precursor injection into the stratosphere was small or short-lived. Since our station is at the same latitude as the volcano, maximum loading would be expected in the stratospheric layer sampled by this photometer. Because the loading is undetected in this zone, no long-term effect on weather would be expected due to stratospheric loading by Mt. St. Helens.

4. Summary

Observations of the direct solar beam attenuation some 200 km from Mt. St. Helens to quantify the amount and size of aerosols before and after the six major eruptions of 1980 were presented. The major conclusions are two: based on our comparison of 1980 and earlier attenuation data, Mt. St. Helens produced no substantial perturbation to the aerosol load in the stratosphere, and the SO_2 to sulfate aerosol conversion in the troposphere proceeded on several occasions at a much accelerated rate compared to that of most anthropogenic SO_2 sources.

We originally considered Mt. St. Helens as a model for SO_2 to sulfate conversion, i.e., a scaled-up pollution source. Since Mt. St. Helens was far and away

the largest single producer of SO_2 (and a rather isolated one at that) in the Pacific Northwest during 1980, it would have served our purposes nicely in that a clear signal was to be expected. A faster SO_2 to sulfate conversion rate has been observed and seems to preclude making Mt. St. Helens a representative model of sulfur conversion processes associated with anthropogenic activity.

Acknowledgments. The authors wish to thank Nels Laulainen for a careful reading of the manuscript and helpful suggestions for its improvement. Ed Kleckner and John Schmelzer provided computer assistance, and Bob Kerns and Monte Orgill assisted in the trajectory analysis for which we are appreciative. This work was supported by the Office of Basic Energy Sciences within the Department of Energy under Contract DE-AC06-76RLO 1830.

REFERENCES

Alkezweeny, A. J., and D. C. Powell, 1977: Estimation of the transformation rate of SO_2 to SO_4 from atmospheric concentration data. *Atmos. Environ.*, **11**, 179–182.

Angstrom, A., 1961: Techniques of determining the turbidity of the atmosphere. *Tellus*, **13**, 214–223.

Bevington, P. R., 1969: *Data Reduction and Error Analysis for the Physical Sciences.* McGraw-Hill, 336 pp.

Casadevall, T. J., D. A. Johnston, D. M. Harris, W. I. Rose, Jr., L. L. Malinconico, R. E. Stoiber, T. J. Bornhorst, S. N. Williams, L. Woodruff and J. M. Thompson, 1981: SO_2 emission rates at Mount St. Helens from March 29 through December 1980. U.S. Geological Survey, Prof. Pap. No. 1250, 193–200.

Crutzen, P. J., 1976: The possible importance of CSO for the sulfate layer of the stratosphere. *Geophys. Res. Lett.*, **3**, 73–76.

Hansen, J., D. Johnson, A. Lacis, S. Lebedeff, P. Lee, D. Rind and G. Russell, 1981: Climate impact of increasing atmospheric CO_2. *Science*, **213**, 957–966.

Junge, C. E., 1963: *Air Chemistry and Radioactivity.* Academic Press, 382 pp.

——, C. W. Chagnon and J. E. Manson, 1961: Stratospheric aerosols and climate. *J. Meteor.*, **18**, 81–108.

Kleckner, E. W., J. J. Michalsky, L. L. Smith, J. R. Schmelzer, R. H. Severtsen and J. L. Berndt, 1981: A multipurpose computer-controlled scanning photometer. Pacific Northwest Laboratory, PNL-4081, 31 pp.

Peterson, J. T., E. C. Flowers, G. J. Berri, C. L. Reynolds and J. H. Rudisill, 1981: Atmospheric turbidity over central North Carolina. *J. Appl. Meteor.*, **20**, 229–241.

Pollack, J. B., 1981: Measurements of the volcanic plumes of Mount St. Helens in the stratosphere and troposphere: introduction. *Science*, **211**, 815–816.

Toon, O. B., and J. B. Pollack, 1980: Atmospheric aerosols and climate. *Amer. Sci.*, **68**, 268–278.